16th World Conference on Earthquake, 16WCEE 2017
Santiago Chile, January 9th to 13th 2017
Paper N°1306
Registration Code: S-C1464733306

Numerical Modeling of Self-centering Steel Plate Shear Walls

X.Y. Wang[(1)], W.S. Lu[(2)], J.P. Han[(3)]

[(1)] Ph. D. candidate, College of Civil Engineering, Tongji University, Shanghai, China. E-mail: wxyjennifer@163.com
[(2)] Professor, College of Civil Engineering, Tongji University, Shanghai, China. E-mail: wally@tongji.edu
[(3)] Professor, School of Civil Engineering, Lanzhou University of Technology, China. E-mail: jphan@lut.cn

Abstract

The self-centering steel plate shear wall (SC-SPSW) is a new seismic load-resisting system that combines the steel plate shear walls (SPSWs) and the post-tensioned (PT) beam-to-column connections. It has strong lateral load resistance, high energy dissipation and good recentering capability. Numerical model with continuum elements is proposed since it is of importance for capturing the detailed behavior of SC-SPSW and investigating the effects of various parameters on web plate and PT connection behaviors. The calculated responses of models including hysteresis response, PT force, PT connection axial force and moment, web plate shear resistance are compared with the experimental data to validate the modeling method. The results present a good agreement in the system performance and the numerical model is able to account for more complex web plate behavior, including the web plate stress and strain development. Furthermore, this study proves that the thicker web plate increases the PT connection and boundary frame demands and has a negative impact on the PT force. The compressive stress in web plate increases with the increasing web plate thickness. And the compressive stress has an increasing trend after the web plate full yielding under the cyclic load. The research provides an effective modeling method for the parametric study on the SC-SPSW performance.

Keywords: self-centering; web plate; PT connection; numerical model; compressive stress

1. Introduction

Self-centering steel plate shear wall (SC-SPSW) system is a high performance load-resisting structural system which combines the advantages of steel plate shear walls (SPSWs) and the post-tensioned (PT) beam-to-column connection. Under lateral loading, the steel plate shear wall referred to as web plates, can dissipate energy and provide high stiffness and strength through developing tension-field action, whereas the PT connection between beam and column can provide the restoring force for the whole structure. SC-SPSW is intended to reduce residual drift and structure damage to beam (horizontal boundary element, HBE) and column (vertical boundary element, VBE) in the conventional SPSW and reduce repair costs and loss of functionality in a building after an earthquake.

The research on SC-SPSW starts from the project NEES-SG: Smart and Resilient Steel Plate Shear Walls for Reducing Earthquake Impacts. A group of researchers have investigated the design philosophies [1, 2, 3] and done the experimental and numerical simulation study of SC-SPSW. The experiments consist of three parts：large-scale quasi-static subassembly tests，third-scale quasi-static and shaking table tests and full-scale pseudo-dynamic tests[4, 5, 6]. To understand the overall system behavior of SC-SPSW, the quasi-static subassembly experiments are clearly described in [4], which including four, two-story specimens and investigated the impact on response of two parameters: the number of post-tensioning strands used in PT connection, and the web plate thickness. With regard to the numerical studies, Clayton et al. have presented different methods of modeling SC-SPSWs [7]. The strip models in OpenSees, employed nonlinear springs in the PT connection to simulate the rocking behavior and a diagonal strip model to simulate the web plate, were primarily investigated, as the tension-compression strip model was shown to better at predicting the reloading and unloading strengths of the SC-SPSWs [8, 9, 10]. However, when it is necessary to research the complex behavior of the web plate, the shell element web plate model is more appropriate to utilize.

To investigate the web plate behavior that can't be captured in the experiments and to provide a modeling method for the future parametric study of the web plate, the focus of this paper is to develop the SC-SPSW modeling method in ABAQUS. According to the quasi-static subassembly tests, the four specimens are modeled and analyzed under monotropic load and cyclic load. The system general response, PT connection and web plate responses of the models are compared with the experimental results for evaluating the modeling method. Furthermore, the detailed behavior of the SC-SPSW, including the PT force, the PT connection moment and the stress and strain developments of the tension field action in web plate, are significantly explained.

2. Description of Model

Four SC-SPSW numerical models that are single-bay two-story frames with in-filled thin steel plate walls were built. These models correspond to the experimental specimens that were named 6s75k20Ga, 8s100k20Ga, 6s75k16Ga and 8s100k16Ga, respectively. The naming scheme identifies the number of strands used in the PT connection (6s or 8s), the initial total PT force in units of kips (75k or 100k), and the web plate gauge thickness (16Ga or 20Ga). The details of the experiments were fully described in [4]. Identical with the test setup, the south VBE is pinned and the north VBE base is constrained by roller at the base through constraining the reference points. The overall model of one specimen is shown in Fig. 1. The models are 3235mm wide from VBE centerline-to-centerline, with the height of 1724mm from HBE centerline-to-centerline, and 4178mm from the center of pin to loading point. In these models, solid elements are used to simulate the boundary frame elements, truss elements are used to simulate the PT strands, and S4R shell elements are used to simulate the web plates. All of the beams are connected to the columns by PT connection models. Because the boundary elements and PT strands were designed to remain elastic, the boundary frame and the PT strands were modeled using the elastic materials with the elastic moduli 200 Gpa and 196.5 Gpa, respectively. Tie constraints are used to connect the edge of the web plate to the boundary elements. The web plates above and below the middle HBE are same thick for each model and the web plate material properties were shown in Table 2 in [5].

The significant difference in the modeling of SC-SPSW and SPSW is the beam-to-column connection. In SC-SPSW modeling, contact interactions between the HBE end flanges and the VBE flange face were employed

to simulate the PT connection rocking behavior, and rough and hard contact behavior were defined to allow the interfaces to separate. The slot connector similar to the horizontally-slotted holes used in the shear tab connections at the beam ends, was built to transfer shear forces in the PT beam-to-column connections while allowing the connection to rock open. The PT members are modeled as truss elements that align with the centroid of each PT group on each side of the beam web and the initial stress is loaded by defining the predefined field of temperature. The model also includes the continuity and reinforcement plates that were present in the test specimen. The boundary frame members and reinforcing plates are modeled using solid element with edge lengths of approximately 50 mm. Also, out-of-plane restraint is provided along the length of each HBE such that only in plane movement of the model occurs.

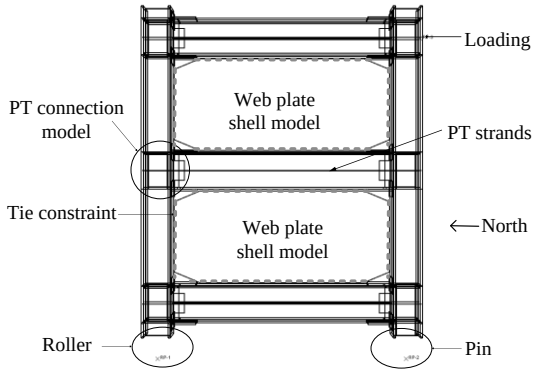

Fig. 1 – Schematic of ABAQUS model

The web plate was modeled using S4R elements. The web plate material was defined approximately using bi-linear material model according to the stress-strain curves in the coupon tests, and pure isotropic hardening was used to define the web plate hardening property according to Webster's previous study [11]. As the initial geometric imperfection of the web plate has influence on its behavior, the web plate shell elements were seeded with small initial out-of-plane imperfections from a buckling analysis, with approximate peak amplitudes of 2.8 mm. The web plate was meshed to elements approximately 50x50 mm. To accurately capture inelastic out-of-plane bending behavior of web plate, nine Gauss integration points were used through the thickness of the shell.

For each specimen, the numerical analyses were performed including pushover analysis and cyclic analysis. All of the simulations employed explicit dynamic analysis in ABAQUS/Explicit. Loads were applied using displacement control of a reference point coupling with some area of the column face. The maximum monotropic displacement reached to 4% drift. The displacement amplitude history of the cyclic loading comprised one cycle at target peak drifts of 0.117% ($1/3\,\delta_y$), 0.233% ($2/3\,\delta_y$), 0.35% (δ_y), 0.7% ($2\,\delta_y$), 1.05% ($3\,\delta_y$), 1.5%, 2%, 2.5%, 3%, and up to 4%. δ_y is corresponding to the yield deformation of the specimen.

3. Comparison of Response

3.1 General response

The SC-SPSW response is theoretically characterized by the PT connection decompression and web plate yielding. Take 8s100k20Ga model as example, the key points in the push-over and cyclic responses are illustrated in Fig.2. The red line is the backbone curve of specimen 8s100k, which is the PT frame without web plates. Point A corresponds to decompression at the PT connection. As the moment at the connection surpasses the decompression moment, a gap opens on the tension side of the HBE and the PT connection rocks. The stiffness between Points A and B is provided by the elastic tension field in the web plate and the post-decompression stiffness of the PT frame. Point B identifies full yielding of the web plates. From this point on the lateral stiffness will be primarily provided by the post decompression stiffness of the PT frame and strain hardening in the web plates. This is the onset of energy dissipation by the web plates. Noted that the hysteretic curves don't have strength degradation phase due to damage in the web plates are not simulated in the models. In the hysterestic curve, points C through F also can be identified. Point C identifies unloading of the web plate

tension field and marks the onset of web resistance via compression and shear. The web plate compressive and shear strength results from plastic deformation and kinking of the web plate and the associated geometric stiffness and strength. Point D indicates the development of the full compressive or shear strength of the plate. Point E indicates the recompression of the PT connection. Point F identifies redevelopment of tension field strength during re-loading following cycles of web plate yielding. In addition to that the bare frame curve can help identify two significant points (Point A and Point C), after the PT connection decompression, the portion of the SC-SPSW hysteretic curve above the bare frame response approximately represents web plate contribution due to the tension field, and the portion of the hysteretic curve below the bare frame response represents the contribution of the compressive strength of the web plate [4].

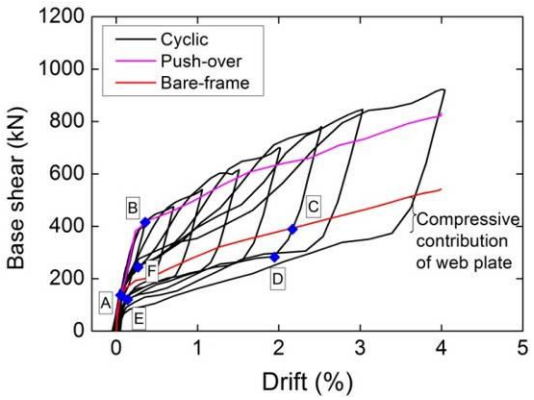

Fig.2 – Significant points in SC-SPSW responses

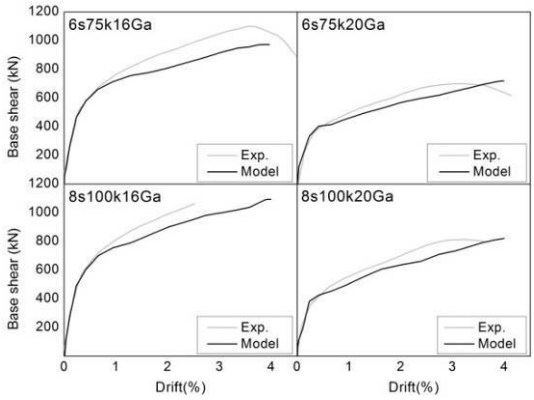

Fig. 3 – Comparison of model pushover curves and experimental skeleton curves

In Fig. 3, the numerical pushover curves are compared with the positive portion of the experimental skeleton curves for each specimen. The stiffness of the simulative curve closely matches the stiffness of experimental curve before the web plate yielding. After the web plate yielding, the hysteretic envelops of each specimen significantly exceed the pushover capacity curves because of the nature of the hardening exhibited by the web plate materials. And the extent of the hardening increases with the increasing thickness of web plate. The hardening property defined in the model has been shown to significantly impact the web plate capacity and reloading behavior in [11] and the results also show that the isotropic hardening should be assumed for A1008 plate, which will be applied in SC-SPSW study.

Then to understand the SC-SPSW hysteresis, the results of the cyclic analysis are compared with the test data from the experiments in Fig. 4, showing the model responses are in good agreement with the experimental responses before the strength degradation occurs in experiments. Since the models can't simulate the system damage, the responses before the web plates damage are only compared and investigated. Fig. 4(b) shows the hysteretic envelops from the numerical analyses and the experimental responses. In the positive direction (when push the specimen), the envelops of the models accurately predict the actual behavior, while in the negative direction the tests show a some premature softening near the yield point where the experimental curves dip under the simulated curves. It is believed this is due to the asymmetric stiffness in the PT response and the asymmetry is more easily detected in the simulation, this will be discussed in the PT connection behavior. For clarity, the numerical and experimental behavior for specimen 8s100k20Ga subjected to cycle at 2% drift only are compared in Fig. 5. The characteristics of the unloading and reloading behavior for a cycle prior to web plate tearing can be captured by comparing the key points of hysteretic behavior. The figure indicates that the model overestimates the strength during reloading (Point F) and underestimates the web plate resistance during unloading (Point D). But their energy dissipation is approximate. The overestimation of the reloading strength is believed to be due to web plate strain hardening in the isotropic hardening model, minor damage in the specimen web plate that was not simulated in the models. Also, the residual drift of the model is underestimated, which indicates that the recentering capability of the system is overestimated. Therefore, the overestimation of the reloading strength is also induced by the overestimation of PT force. Whereas the underestimation of web plate unloading resistance is believed to be concerned with the underestimation of the web plate shear strength and substantially, the difference of the web plate compressive stress development between the test and the simulation.

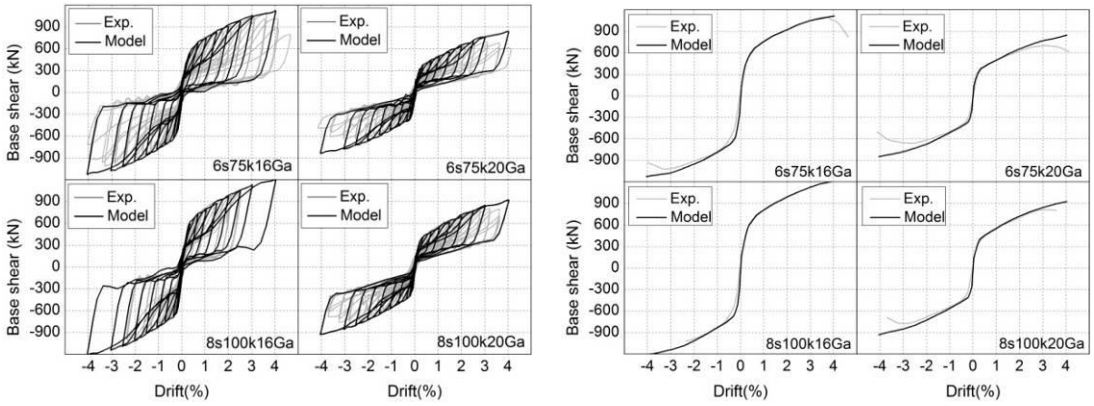

(a) (b)

Fig. 4 – Hysteretic responses of models and experiments: (a) Hysteretic curves and (b) Skeleton curves

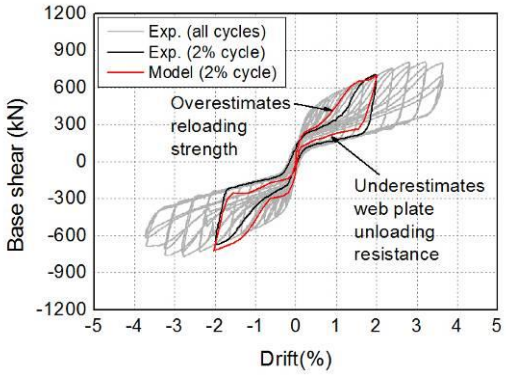

Fig. 5 – Comparison of experimental and numerical responses at 2% drift cycle of specimen 8s100k20Ga

3.2 PT Connection response

The PT connection provides recentering force for the SC-SPSW through the elongation of the PT strands as the connection gap opens. The PT force response at a connection correlates with the capability of the system recentering. Under the laterally loading, the response of the PT strands begins with initial prestress and the PT force increases linearly as the connection decompresses and the connection rotation increases. It is noted that the distance between the column centerlines is increasing as the connection gaps open, this phenomenon is denoted as frame expansion in [12]. To accommodate the frame expansion, roller at the north VBE base is employed.

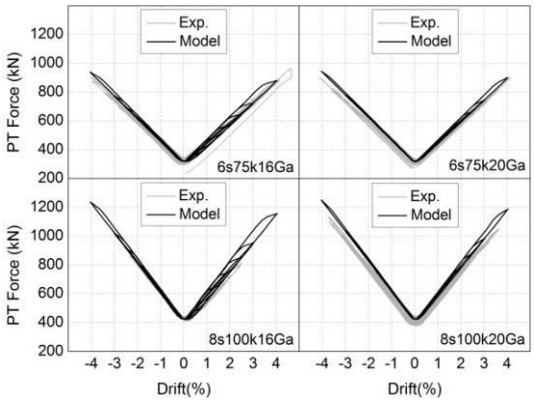

Fig. 6 – Comparison of PT forces at the middle HBE

In Fig. 6, the cyclic responses of the PT strands at the middle HBE from the simulation and the tests are compared, showing that the PT forces are slightly overestimated and the PT stiffness is asymmetric. The PT

stiffness is larger in the negative direction than that in the opposite direction, subsequently, it contributes to the system overall stiffness is larger, as shown in Fig. 4(b). In addition, some hysteretic area in the PT response is observed in model. As the PT strands and the boundary frame remain elastic under full loading, the hysteretic area is due to the slip at the roller (shown in Fig. 1) rather than the yielding of the PT strands. It is also noted that the limited hysteretic area in the PT response at the positive direction is larger than that at the negative direction. The amount of the area increases for increasing the thickness of the web plate. This indicates that the roller slips are different under loadings from different directions and the thicker web plate causes a larger slip displacement (e.g. the max slip for 8s100k16Ga is 27.4 mm and the max slip for 8s100k20Ga is 25.2 mm at 4% drift in the simulative results).

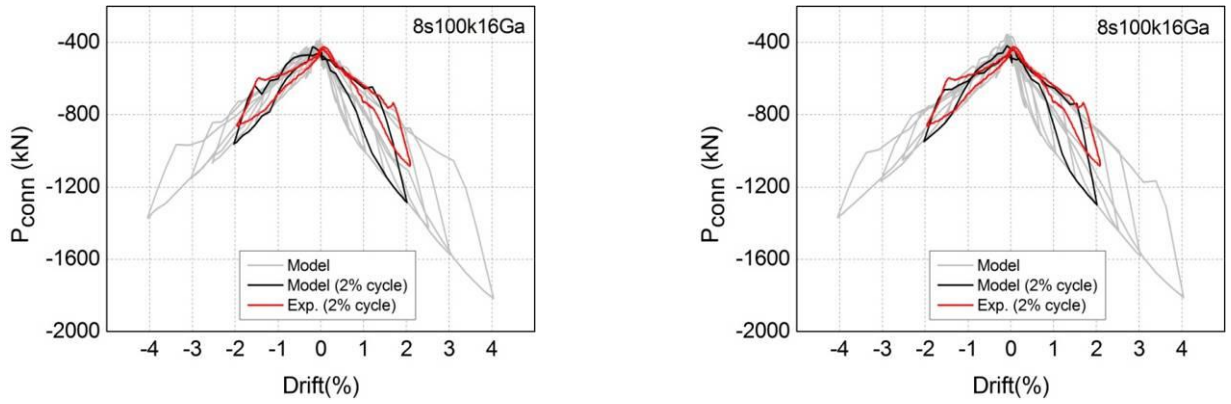

(a) (b)

Fig. 7 – Connection axial force demand (a) at north and (b) south connection for Specimen 8s100k16Ga

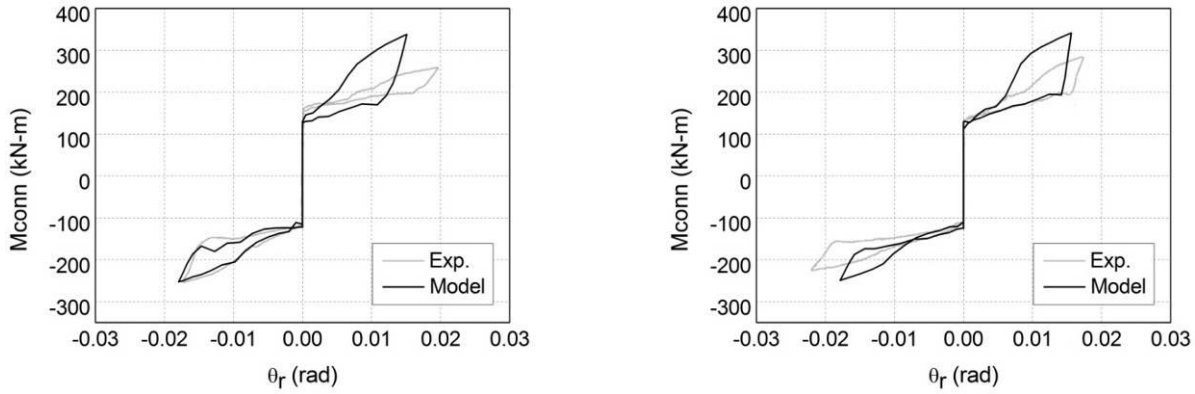

(a) (b)

Fig. 8 – Comparison of (a) north and (b) south connection moment response at the 2% drift cycle for Specimen 8s100k16Ga

The modeling method proposed here is able to be used to directly acquire the axial force and moment of the two ends of HBEs through the contact forces between the ends of the HBE flange and the VBE flange face, subsequently, to determine the PT connection moment [1]. The connection rocking point is the extreme fiber of the flange reinforcing plate is assumed. Also, the relative rotation of the connection can be directly attained from the output of the slot connector combined with cardan. For comparing with the experimental results in [5], Fig. 7 and Fig. 8 show the numerical and experimental comparisons of axial force and moment demand at 2% drift, respectively, for the north connection and the south connection in the middle HBE in specimen 8s100k16Ga. The responses of the two connections in the model overestimate the experimental measured responses, especially in the positive direction. Dowden et al. have presented that the axial force at HBE ends includes PT force (T_s), the pull-in force of the VBEs ($P_{HBE(VBE)}$) and the web plate force along the HBE ($P_{HBE(web)}$) in [1]. Thus, the overestimation in the connection axial demands is primarily believed to be due to the overestimation of the PT

force, as shown in Fig. 6, and the overestimation of the web plate reloading strength that results in the overestimation of $P_{HBE(VBE)}$ and $P_{HBE(web)}$. Otherwise, the axial force from the experiments is extrapolated under some assumptions so that there is some difference from the simulation results. Similar to the axial force demand, the connection moment demand is also overestimated, shown in Fig. 8(b). Furthermore, due to the different slips of the roller at the positive direction and the negative direction (e.g. the max slips for 8s100k16Ga at positive and negative directions of 2% drift are 16mm and 5mm respectively in model), the connection responses ($P_{conn}, M_{conn}, \theta_r$) are asymmetric in the two directions, and more overestimation of the roller slip at the positive direction results in larger loop area of the connection response, which can also be verified in Fig. 6.

Therefore, the general trend of the PT connection behavior in the simulation is consistent with the trend in the tests, although the models overestimate the axial force and moment demands of the PT connection and overestimate the slips occurred at the north VBE base in the positive direction. Neglect the effect of the slip on the PT connection hysteretic response, the models are able to reasonably predict the PT connection behavior in SC-SPSW.

3.3 Web plate behavior

Web plate behaves as the energy dissipation component and contributes significant initial stiffness and strength for the SC-SPSW. It resists lateral loading through tension field action and dissipate energy through yielding in the direction of the tension field. And the web plates have some compressive strength that should be concerned because it has an impact on lateral strength and the recentering capability of SC-SPSW. The shell element model is applied to investigate the complex web plate behavior. The tension-field action including the orientation of buckling waves in plates and the web plate stress and strain distribution are able to be approximately modeled.

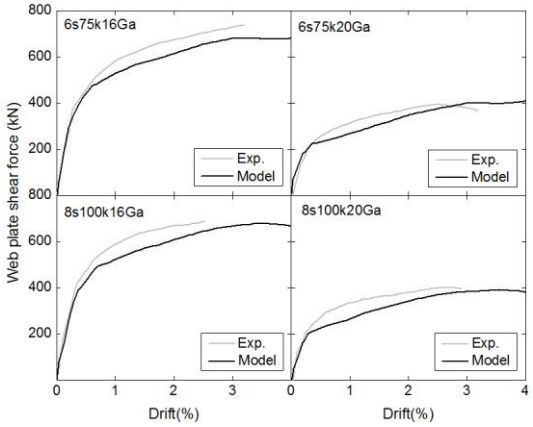

Fig. 9 – Comparison of web plate shear force resistance

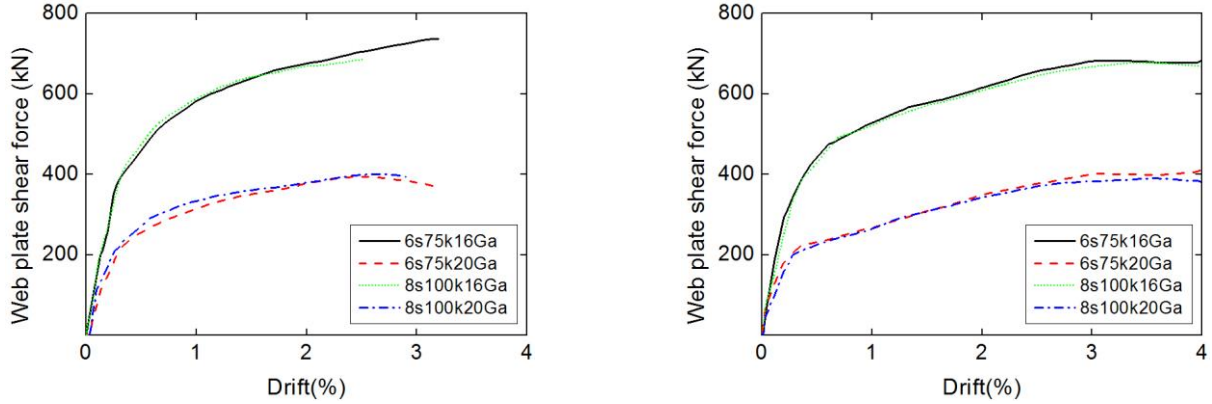

(a) (b)

Fig. 10 – Web plate shear resistance of (a) experiments and (b) models

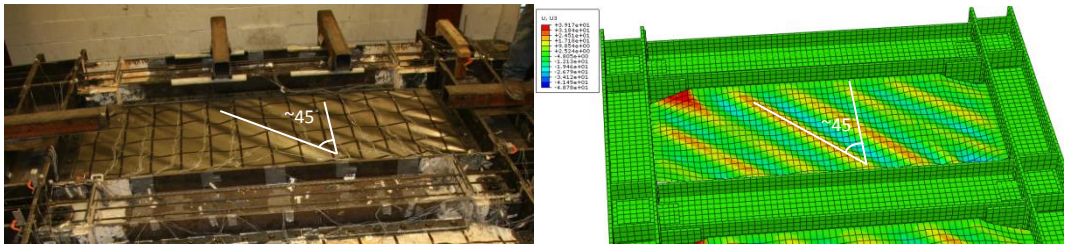

(a) (b)

Fig. 11 – Comparison of web plate responses at 2% drift in (a) experiment (b) shell element model for specimen 8s100k20Ga

As the SC-SPSW overall system response is a combination of the responses of PT boundary frame and the web plates. The web plate shear force resistance in the system is able to be equivalently attained by subtracting the bare frame shear from the system base shear. Fig. 9 compares the equivalented web plate shear forces of the models and the experiments for each specimen, respectively. It is found that the web plate shear strength is underestimated after the web plates yielding, but the initial stiffness of the web plates is closely simulated. Reasonably, models with thicker web plates are able to resist lager shear force under laterally load. Noted that the extent of the shear strength underestimation is similar for the same thick web plates and the web plate strength capabilities in models and experiments have an identical variation trend, shown in Fig. 10. Thus, the modeling method is still able to predict the effects of the parameters on the web plate performance.

The web plate strength underestimation also includes the underestimation of the compressive strength, which induces the underestimation of the system unloading resistance for the cyclic behavior, seen in Fig. 5. The discrepancy is attributed to the simulation can't fully copy the development of tension field in the experiments. This can be validated in Fig. 11 through an overview of buckling waves for specimen 8s100k20Ga at 2% drift. The number of the buckling waves in experiment reached 11, with the amplitude of the waves approximately 38 mm, whereas the number of the buckling waves in the model is 9, with the max amplitude of the waves about 40 mm. These differences between the models and the experiments result from that some phenomena, such as slips of the web plate corners at the fish plate connection, the web plate kinking and tearing near the corners, are not simulated in the models, but they can have an effect on the whole web plate strain and stress distribution and result in more buckling waves and the higher shear strength in the web plates. So the development of web plate strength in model is different from the experimental results. Additionally, both in the experiment and in the model, the orientation of the buckling waves from the vertical is about 45 degree, which is consistent with the assumed inclined angle.

3.4 Model evaluation

The model responses including hysteresis behavior, PT force response, PT connection rotation and moment, and web plate strength capability are analyzed and compared with the experimental results to evaluate the model in this study. These comparisons verified that the models are able to agree with the experiments. In general, the hysteresis behavior in model is well approximate with the experimental hysteresis and the models can be used to predict SC-SPSW performance before the web plate damage occurs. In particular, the model overestimates the reloading strength and underestimates the web plate shear and compressive strength during unloading. For details, the PT force and the PT connection axial force and moment demands are overestimated due to the PT force losses are not simulated. While the web plate strength is underestimated, which is ascribed to the discrepancy of tension filed formation between the simulation and the actual behavior. Even so, the PT connection and web plate behavior variation trends keep consistent with the experimental responses, and the model is appropriate for investigating the parametric study of the SC-SPSW.

4. Parameric Analysis of SC-SPSW Response

The design parameters included web plate thickness, t_w, number of PT strands, N_s, and total initial PT force, T_0, has been investigated in the quasi-static cyclic experiments[4, 5]. The results showed that the specimens with

more PT strands and larger initial PT forces had lower residual drifts and, therefore, better recentering capabilities. The specimens with thicker web plates had larger strength and energy dissipation. But the thicker web plate in the system induced worse recentering capabilities owing to the compression resistance of web plate during unloading. This influence is neglected in the design assumptions proposed by Clayton et al.[10]. Although the experiments can identify the effect that the web plate compression resistance had on the SC-SPSW performance, it is hard to be directly measured and quantified. Thus, the modeling method is employed in this study to presents the system detailed responses, such as the HBE axial force, the web plate stress and strain disstribution, which are significant but difficult to be directly captured in the experiments. The impacts of the varied parameters, t_w, N_s and T_0, on the SC-SPSW response are explained.

Fig. 12 shows the comparison of the model responses under monotropic load. The values of the stiffness for the models are also caculated in Table 1. K_1 is the initial stiffness and is a combination of the elastic tension field stiffness of the web plate and the pre-decompression stiffness of the PT frame. K_2 is the system stiffness just after connection decompression and combines the elastic tension field stiffness with the decreased PT frame stiffness following decompression. K_3 is the combination of the post-decompression stiffness of the PT frame and the post-yield strain hardening stiffness of the web plate. It is found that increasing the number of PT strands increases the stiffness and strength of the system in full loading process. When the number of PT strands increases from 6 strands to 8 strands, K_1, K_2 and K_3 have an increase of about 6%, 7%, and 22%, respectively. This indicates that the effect of the PT strands on the initial stiffness is small and after the web plates yielding the number of PT strands variation in system response is noticeable. Additonally, When the web plate thickness increases from 0.92 mm to 1.52 mm, K_1 has an increase of about 35%, K_3 almost has no increase. It verifies that increasing the thickness of web plate significantly increases the system initial stiffness. Furthermore, from PT force versus drift responses of the models in Fig. 12(b), it was also found that the web plate thickness has no effect on the PT stiffness due to that the curves of the models with different thickness of web plate are parallel. But the maganitude of the PT force is lower when the model has thicker web plate.

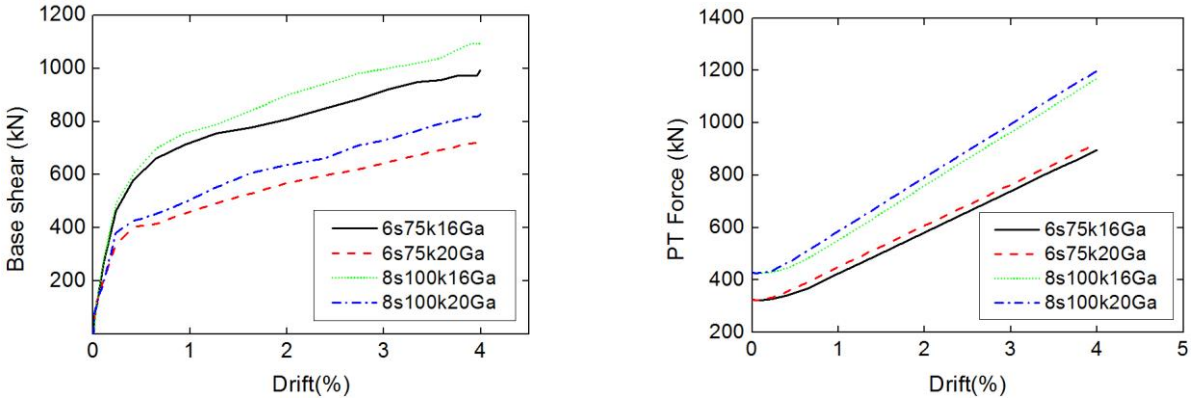

(a) (b)

Fig. 12 – (a) Base shear versus drift response and (b) PT force versus drift response of the models under monotropic loading

Table 1 – Comparison of the system stiffness for the models

Models	K_1 **(kN/m)**	K_2 **(kN/m)**	K_3 **(kN/m)**
6s75k16Ga	48182	8428	2198
6s75k20Ga	34862	4453	2238
8s100k16Ga	51096	9061	2664
8s100k20Ga	38096	5851	2690

To show the effects of the parameters on the PT connection behavior, the connection moment (M_{conn}) versus rotation (θ_r) response for each model is shown in Fig. 13. Models with same number of PT strands are expected to decompress with the same connection moment. The connection moment increases for increasing the number of PT strands. While the PT force is slightly negatively affected by the web plate, increasing the web plate thickness still results in the increasing of the connection moment, this implies the connection and the boundary frame demands are significantly correlated with the web plate. As such, the connection moment that equals the total PT force (T_s) is multiplied by half the HBE depth in [1], significantly underestimate the boundary frame demands. The figure also indicates that after the connection decompression, the PT connection stiffness varies with the variation of the thickness of the web plate, but after the web plate yielding, the effects eliminate.

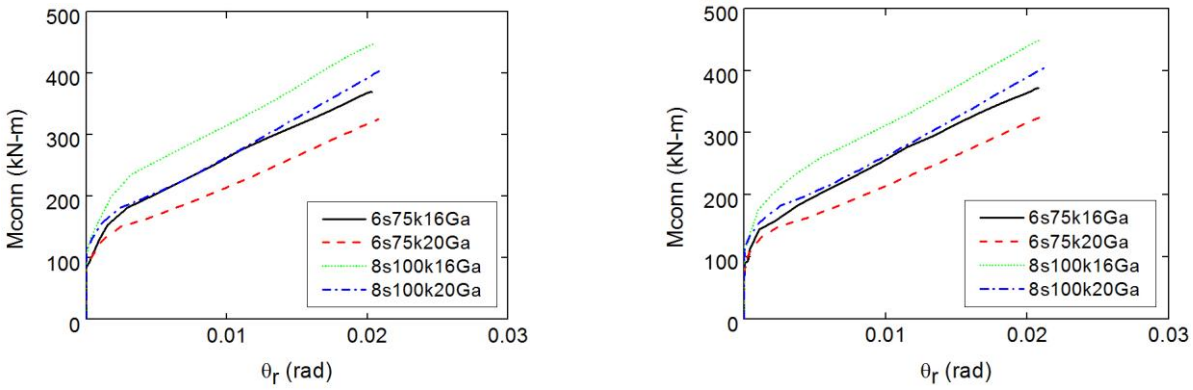

Fig. 13 – Moments of (a) north and (b) south connection in the middle HBE of the models

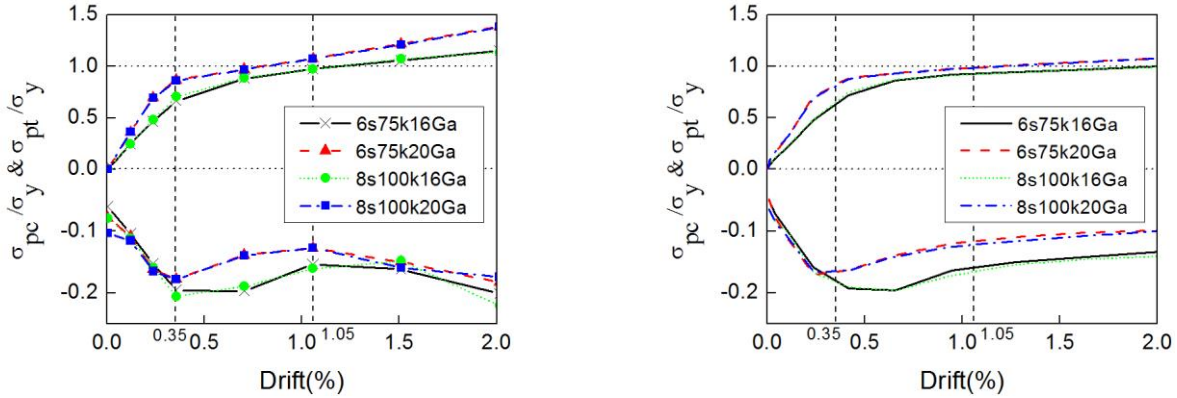

Fig. 14 – Mean nominal principal stresses (σ_{pc} & σ_{pt}) normalized by plate nominal yield stress (σ_y) (a) under the cyclic load and (b) under the monotropic load

The web plate behavior is characterized by the tension field action and the experimental results have proved that there is non-negligible compressive strength in the web plate. The web plate principal stresses are easier extracted from the models than be measured through strain measurement in an experiment. The relative magnitudes of the mean principal tensile stress and mean principal compressive stress in the web plate under cyclic load and monotropic load, normalized by the plate yield strength are shown in Fig. 14. In Fig. 14(a) the principal stresses are plotted only at the peak of each half-cycle. Reasonably the web plate tensile stress increases with the increasing drift. While the mean principal tensile stress in the thicker web plate is lower at the same drift level. It is attributed to that the thicker web plate has less strain.

Note that the compressive stress of the web plate is approximately 10%-20% of the web plate tensile yield strength. This is identical with the experimental data. Generally, the compressive stress in the web plates increases for increasing the web plate thickness, but its variation with the loading drift is complex. Upon the cyclic loading, the magnitude of the compressive stress increases other than from 0.35% to 1.05% drifts. Note that drift 0.35% correspondes to the system yield drift, δ_y. The system yielding progressively occurs around 0.35% to 1.05% drifts. In this phase, the system compressive stresses are changing to tensile stresses. Therefore, the web plate compressive stress first increases with the increasing drift during the elastic phase, then decreases during yielding occurs progressively over the web plate. The changing trend before 1.05% drift under the cyclic load is similar with that under the monotropic load. However, after 1.05% drift, under the monotropic load the compressive stress continues to decrease, whereas under the cyclic load the trend turns to increases. This is thought to correlate with the accumulated plastic strain of web plate, as shown in Fig. 15. 6s75k16Ga-M and 6s75k16Ga-C seperately identifies the models under monotropic load and cyclic load. The convention is also suitable to other models. The mean accumulated plastic strain under the cyclic load is significantly larger than that under the monotropic load. The amount of the mean accumulated plastic strain near 1.05% drift under the cyclic load has exceeded the amount at 2% drift under the monotropic load. Under the lateral load, with the formation of the tension field, web plate compressive stress becomes to tensile, however when the web plate deformation is large, the compressive stress would increase in order to stabilize the tension field buckling. In Fig. 14(b) the web plate accumulated plastic strains of the models under monotropic load during 0.35% to 2% are in fact corresponding to the strains during drift 0.35% to 1.05% under cyclic load. So the compressive stresses of the web plates behave the tendency of reducing in this extent of drift. In all, the web plate compressive strength tend to increase after the web plate full yielding under the cyclic load. This feature is critical and have an influence on the SC-SPSW hysteretic behavior, because it will increase the system energy dissipation and residual drift.

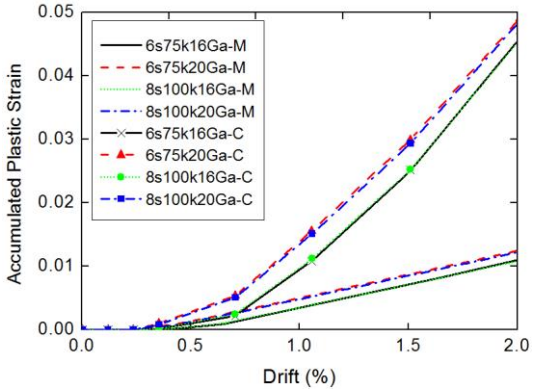

Fig. 15 – Accumulated plastic strain of web plates

5. Conclusions

Models of SC-SPSW using shell elements to simulate the web plate and solid elements to simulate the boundary frame were built in this study. The simulations showed a good agreement with the experimental results. The PT force was slightly overestimated, which resulted in the overestimation of the PT connenction axial force and the moment responses in some extent. The web plate strength was underestimated as some web plate damage, which has effects on the tension field action, was not simulated in the models. Nonetheless, the model accurately predicted the initial stiffness and the strength of the system before web plate damage occured. The variation in the system responses of the models were consistent with the experimental results when impacted by the various parameters. Except that, the complex behavior of PT connection and web plate were capable to directly acquired from the simulation models. Thus, this study provides an effcetive modeling method for the SC-SPSW parametric study in the future.

The effects on the model responses of the parameters: the number of PT strands at each HBE-to-VBE connection and the thickness of the web plates were also explained. The results showed that increasing the web

plate thickness increased the PT and boundary frame demands owing to the connection moment was affected by the web plate thickness. In addition to the web plate had a negatively impact on the PT force response. There was non-negligible compressive strength in the web plate and the thicker web plate had higher compressive stress. Of more important is that the web plate compressive strength is related to the accumulated plastic strain in web plate. When the accumulated plastic strain in web plate is large enough, the web plate compressive stress will increases and amplify its effects on the system seismic performance. Further research is required to quantify the impacts of the parameters on the system responses.

6. References

[1] Dowden DM, Purba R, Bruneau M (2012): Behavior of self-centering steel plate shear walls and design considerations. *Journal of Structural Engineering*, **138** (1), 11-21.

[2] Clayton PM (2010): Self-centering steel plate shear walls: Development of design procedure and evaluation of seismic performance. *Master dissertation*, University of Washington, Seattle.

[3] Clayton PM, Berman JW, Lowes LN (2012): Seismic design and performance of self-centering steel plate shear walls. *Journal of Structural Engineering*, **138** (1), 22-30.

[4] Winkley TB (2011): Self-centering steel plate shear walls: Large scale experimental investigation. *Master dissertation*, University of Washington, Seattle.

[5] Clayton PM, Winkley TB, Berman JW, Lowes LN (2012): Experimental Investigation of Self-Centering Steel Plate Shear Walls. *Journal of Structural Engineering*, **138**, 952-960.

[6] Clayton PM , Dowden DM, Li C-H, Berman JW, Bruneau M, Lowes LN, Tsai K-C(2013): Full-Scale Testing of Self-Centering Steel Plate Shear Walls. *Structures Congress 2013*, 1694-1700.

[7] Clayton PM, Tsai C-Y, Berman JW, Lowes LN (2015): Comparison of web plate numerical models for self-centering steel plate shear walls. *Earthquake engineering and structural dynamics*, **44** (12), 2093-2110.

[8] Clayton PM, Winkley TB, Berman JW, Lowes LN, Dowden DM, Bruneau M (2012): Numerical and Experimental Studies of Self-Centering Steel Plate Shear Walls. *Proceedings of the 15th World Conference on Earthquake Engineering*, Lisbon.

[9] Clayton PM, Berman JW, Lowes LN (2013): Subassembly testing and modeling of self-centering steel plate shear walls. *Engineering Structures*, 1848-1857.

[10] Clayton PM, Berman JW, Lowes LN (2015): Seismic performance of self-centering steel plate shear walls with beam-only-connected web plates. *Journal of constructional steel research*, **106**, 198-208.

[11] Webster DJ (2013): The inelastic seismic response of steel plate shear wall web plates and their interaction with the vertical boundary members. *PhD dissertation*, University of Washington, Seattle.

[12] Garlock MM, Sauce R, Ricles JM (2007): Behavior and design of posttensioned steel frame systems. *Journal of Structural Engineering*, **133** (3), 389-399.